Appl Phys A (2011) 105:329–339
DOI 10.1007/s00339-011-6617-4

Applied Physics A
Materials Science & Processing

INVITED PAPER

Nanophotonic light-trapping theory for solar cells

Zongfu Yu · Aaswath Raman · Shanhui Fan

Received: 1 March 2011 / Accepted: 15 September 2011 / Published online: 28 September 2011

Abstract Conventional light-trapping theory, based on a ray-optics approach, was developed for standard thick photovoltaic cells. The classical theory established an upper limit for possible absorption enhancement in this context and provided a design strategy for reaching this limit. This theory has become the foundation for light management in bulk silicon PV cells, and has had enormous influence on the optical design of solar cells in general. This theory, however, is not applicable in the nanophotonic regime. Here we develop a statistical temporal coupled-mode theory of light trapping based on a rigorous electromagnetic approach. Our theory reveals that the standard limit can be substantially surpassed when optical modes in the active layer are confined to deep-subwavelength scale, opening new avenues for highly efficient next-generation solar cells.

1 Introduction

Light trapping allows photovoltaic (PV) cells to absorb sunlight using an active material layer that is much thinner than the material's intrinsic absorption length. This then reduces the amount of materials used in PV cells, which cuts cell cost in general, and moreover facilitates mass production of PV cells that are based on less abundant materials. In addition, light trapping can improve cell efficiency, since thinner cells provide better collection of photo-generated charge carriers, and potentially a higher open circuit voltage [1].

The theory of light trapping was initially developed for conventional cells where the light-absorbing film is typically many wavelengths thick [2–4]. From a ray-optics perspective, conventional light trapping exploits the effect of total internal reflection between the semiconductor material (such as silicon, with a refractive index $n \sim 3.5$) and the surrounding medium (usually assumed to be air). By roughening the semiconductor-air interface (Fig. 1a), one randomizes the light propagation directions inside the material. The effect of total internal reflection then results in a much longer propagation distance inside the material and hence a substantial absorption enhancement. For such light-trapping schemes, the standard theory shows that the absorption enhancement factor has an upper limit of $4n^2/\sin^2\theta$ [2–4], where θ is the angle of the emission cone in the medium surrounding the cell (Fig. 1a). This limit of $4n^2/\sin^2\theta$ will be referred to in this paper as the *conventional limit*. This is in contrast to the $4n^2$ limit, which strictly speaking is only applicable to cells with isotropic angular response.

For nanoscale films with thicknesses comparable or even smaller than wavelength scale, some of the basic assumptions of the conventional theory are no longer applicable. Whether the conventional limit still holds thus becomes an important open question that has been pursued both numerically [5–15] and experimentally [16–23]. In this paper, we review our recent work on nanophotonic light-trapping theory where we use a statistical coupled-mode theory that describes light trapping in general from a rigorous electromagnetic perspective [24–26]. Applying this theory, we show that the limit of $4n^2/\sin^2\theta$ is only correct in bulk structures. In the nanophotonic regime, the absorption enhancement factor can go far beyond this limit with proper design.

The paper is organized as follows: in Sect. 2, we review the framework of nanophotonic light-trapping theory; in Sect. 3, we apply the theory to periodic structures; in Sect. 4, we show that the conventional light-trapping limit

Z. Yu (✉) · A. Raman · S. Fan
Ginzton Lab, Stanford University, Stanford, CA, 94305, USA
e-mail: zfyu@stanford.edu

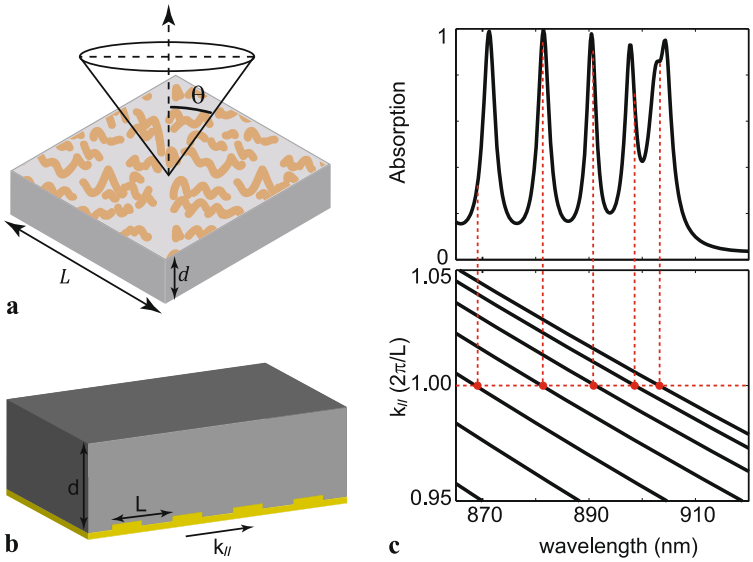

Fig. 1 (**a**) Schematic of light trapping with random texture. (**b**) Light-trapping with the use of a periodic grating on a back-reflector (*yellow*). $d = 2$ μm. $L = 250$ nm. The depth and width of the dielectric groove in the grating are 50 nm and 175 nm, respectively. The dielectric material is crystalline silicon. (**c**) Absorption spectrum (TM mode, normal incidence) and dispersion relation of waveguide modes for the structure in (**b**). The dispersion relation is approximated as $\omega = \frac{c}{n}[(\frac{m\pi}{d})^2 + k_\parallel^2]$, or equivalently in terms of free-space wavelength $\lambda = \frac{2\pi n}{\sqrt{(m\pi/d)^2 + k_\parallel^2}}$, where $m = 1, 2, 3, \ldots$ is the band index indicating the field variation in the transverse direction. Resonances occur when $k_\parallel = 2\pi/L$ (*red dots*)

can be significantly exceeded with the use nanoscale modal confinement; Sect. 5 is the conclusion.

2 Framework of nanophotonic light-trapping theory

To illustrate our theory, we consider a high-index thin-film active layer with a high reflectivity mirror at the bottom, and air on top. Such a film supports guided optical modes. In the limit where the absorption of the active layer is weak, these guided modes typically have a propagation distance along the film that is much longer than the thickness of the film. Light trapping is accomplished by coupling incident plane waves into these guided modes, with either a grating with periodicity L (Fig. 1b) or random Lambertian roughness (Fig. 1a). It is well known that a system with random roughness can be understood by taking the $L \to \infty$ limit of the periodic system [10, 27]. Thus, we will focus on periodic systems. As long as L is chosen to be sufficiently large, i.e. at least comparable to the free-space wavelength of the incident light, each incident plane-wave can couple into at least one guided mode. By the same argument, such a guided mode can couple to external plane waves, creating a guided resonance [28].

A typical absorption spectrum for such a film [6] is reproduced in Fig. 1c. The absorption spectrum consists of multiple peaks, each corresponding to a guided resonance. The absorption is strongly enhanced in the vicinity of each resonance. However, compared to the broad solar spectrum, each individual resonance has very narrow spectral width. Consequently, to enhance absorption over a substantial portion of the solar spectrum, one must rely upon a collection of these peaks. Motivated by this observation, we develop a statistical temporal coupled-mode theory that describes the aggregate contributions from all resonances.

We start by identifying the contribution of a single resonance to the total absorption over a broad spectrum. The behavior of an individual guided resonance, when excited by an incident plane wave, is described by the temporal coupled-mode theory equation [29, 30]:

$$\frac{d}{dt}a = \left(j\omega_0 - \frac{N\gamma_e + \gamma_i}{2}\right)a + j\sqrt{\gamma_e}S. \tag{1}$$

Here a is the resonance amplitude, normalized such that $|a|^2$ is the energy per unit area in the film, ω_0 is the resonance frequency, and γ_i is the intrinsic loss rate of the resonance due to material absorption. S is the amplitude of the incident plane wave, with $|S|^2$ corresponding to its intensity. We refer to a plane wave that couples to the resonance as a *channel*. γ_e is the leakage rate of the resonance to the channel that carries the incident wave. In general, the grating may phase-match the resonance to other plane-wave channels as well. We assume a total of N such channels. Equivalent to the assumption of a Lambertian emission profile as made in Ref. [2], we further assume that the resonance leaks to each of the N channels with the same rate γ_e. Under these assumptions,

the absorption spectrum of the resonance is [29]

$$A(\omega) = \frac{\gamma_i \gamma_e}{(\omega - \omega_0)^2 + (\gamma_i + N\gamma_e)^2/4}. \tag{2}$$

For light-trapping purposes, the incident light spectrum is typically much wider than the linewidth of the resonance. When this is the case, we characterize the contribution of a single resonance to the total absorption by a *spectral cross section*:

$$\sigma = \int_{-\infty}^{\infty} A(\omega)\, d\omega. \tag{3}$$

Notice that spectral cross section has units of frequency, and has the following physical interpretation: For an incident spectrum with bandwidth $\Delta\omega \gg \sigma$, a resonance contributes an additional $\sigma/\Delta\omega$ to the spectrally averaged absorption coefficient.

For a single resonance, from (2) and (3), its spectral cross section is

$$\sigma = 2\pi\gamma_i \frac{1}{N + \gamma_i/\gamma_e} \tag{4}$$

which reaches a maximum value of

$$\sigma_{\max} = \frac{2\pi\gamma_i}{N} \tag{5}$$

in the *over-coupling* regime when $\gamma_e \gg \gamma_i$. We emphasize that the requirement to operate in the strongly over-coupling regime arises from the need to accomplish broadband absorption enhancement. In the opposite narrow-band limit, when the incident radiation is far narrower than the resonance bandwidth, one would instead prefer to operate in the critical coupling condition by choosing $\gamma_i = N\gamma_e$, which results in $(100/N)\%$ absorption at the resonant frequency of ω_0. The use of critical coupling, however, has a lower spectral cross section and is not optimal for the purpose of broadband enhancement. The intrinsic decay rate γ_i differentiates between the two cases of broad-band and narrow-band. For light trapping in solar cells, we are almost always in the broad-band case where the incident radiation has bandwidth $\Delta\omega \gg \gamma_i$.

We can now calculate the upper limit for absorption by a given medium, by summing over the maximal spectral cross section of all resonances:

$$A_T = \frac{\sum \sigma_{\max}}{\Delta\omega} = \frac{1}{\Delta\omega} \sum_m \frac{2\pi\gamma_{i,m}}{N} \tag{6}$$

where the summation takes place over all resonances (labeled by m) in the frequency range of $[\omega, \omega + \Delta\omega]$. In the over-coupling regime, the peak absorption from each resonance is in fact relatively small; therefore the total cross section can be obtained by summing over the contributions from individual resonances. In addition, we assume that the medium is weakly absorptive such that single-pass light absorption is negligible.

Equation (6) is the main result of this paper. In the following discussion, we will first use (6) to reproduce the well-known $4n^2$ conventional limit, and then consider a few important scenarios where the effect of strong light confinement becomes important.

We first consider a structure with period L and thickness d that are both much larger than the wavelength. In this case, the resonance can be approximated as propagating plane waves inside the bulk structure. Thus, the intrinsic decay rate for each resonance is related to a material's absorption coefficient α_0 by $\gamma_{i,m} = \gamma_i = \alpha_0 \frac{c}{n}$. Equation (6) thus can be simplified as

$$A_T = \frac{2\pi\gamma_i}{\Delta\omega} \cdot \frac{M}{N} \tag{7}$$

where M is the number of resonances in the frequency range $[\omega, \omega + \delta\omega]$ given by [31]

$$M = \frac{8\pi n^3 \omega^2}{c^3} \left(\frac{L}{2\pi}\right)^2 \left(\frac{d}{2\pi}\right) \delta\omega. \tag{8}$$

Each resonance in such frequency range can couple to channels that are equally spaced by $\frac{2\pi}{L}$ in the parallel wavevector $k_\parallel$ space (Fig. 2a). Moreover, since each channel is a propagating plane wave in air, its parallel wavevector needs to satisfy $|k_\parallel| \le \omega/c$. Thus, the number of channels is

$$N = \frac{2\pi\omega^2}{c^2} \left(\frac{L}{2\pi}\right)^2. \tag{9}$$

From (7), the upper limit for the absorption coefficient for this system is then

$$A_T = \frac{2\pi\gamma_i}{\Delta\omega} \cdot \frac{M}{N} = 4n^2\alpha_0 d \tag{10}$$

resulting in the upper limit for the absorption enhancement factor F,

$$F \equiv \frac{A_T}{\alpha_0 d} = 4n^2 \tag{11}$$

which reproduces the $4n^2$ conventional limit, appropriate for the Lambertian emission case with $\sin\theta = 1$. The theory can be generalized to the case of a restricted emission cone, and reproduces the standard result of $4n^2/\sin^2\theta$.

The analysis here also points to scenarios where the conventional limit is no longer applicable. Equation (9) is not applicable when the periodicity is comparable to the wavelength, while (8) is not valid when the film thickness is much smaller than the wavelength. Below, we consider both of these cases.

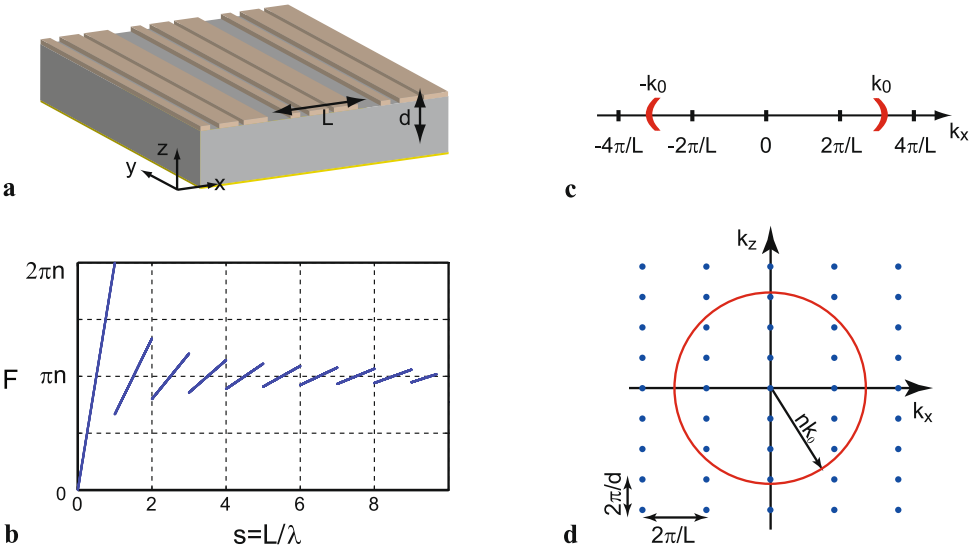

Fig. 2 (**a**) Schematic of a grating structure. *Brown ribbons* are non-absorptive dielectric medium. The whole structure is placed on a perfect mirror (*yellow*). (**b**) Upper limit of absorption enhancement in 1D grating films without mirror symmetry. (**c**) Channels in 1D k-space. (**d**) Resonances in a film with 1D grating. *Dots* represent resonances

3 Light trapping in periodic grating structures

When the periodicity L is comparable to the wavelength λ, the discrete nature of the channels becomes important. To illustrate this effect, we assume that the film has a high refractive index (for example, silicon), such that the wavelength in the material is small compared with the periodicity. We also assume that the film has a thickness of a few wavelengths. In this case, all modes have approximately the same decay rate $\gamma_i = \alpha_0 \frac{c}{n}$, (8) can still be used to count the number of resonances.

3.1 Theoretical upper limit of enhancement factor for 1D grating structures

We first consider a 1D grating defined by structures that are uniform in one dimension, e.g. y-direction, and are periodic in the other dimension (x-direction in Fig. 2a) with a periodicity L. We consider incident light propagating in the xz-plane. We also assume a general case where the grating profile has no mirror symmetry along the x-direction (Fig. 2a). The effect of symmetry will be described later.

For light incident from the normal direction, the periodicity results in the excitation of other plane waves with $k_x = 0, \pm 2\pi/L, \pm 4\pi/L, \ldots$ in the free space above. Moreover, since these plane waves are propagating modes in air, one needs to have $k_x \leq k_0$, where k_0 is the wavevector of the incident light. These two requirements completely specify the number of channels available in k-space (Fig. 2a).

We first consider the case $L \gg \lambda$. The spacing of the channel is $\frac{2\pi}{L} \ll \frac{2\pi}{\lambda} = k_0$. The discreteness of the channels is therefore not important. The total number of channels (Fig. 2c) at wavelength λ thus becomes

$$N = \frac{2k_0}{2\pi/L} = \frac{2L}{\lambda}. \tag{12}$$

Notice that we consider only a single polarization. In the frequency range $[\omega, \omega + \Delta\omega]$, the total number of guided resonances supported by the film is (Fig. 2d):

$$M = \frac{2n^2\pi\omega}{c^2}\left(\frac{L}{2\pi}\right)\left(\frac{d}{2\pi}\right)\Delta\omega. \tag{13}$$

Combining (7, 12–13), we obtain the upper limit for absorption enhancement

$$F = \frac{A}{d\alpha} = \pi n^2. \tag{14}$$

In contrast to the bulk limit of $4n^2$, the enhancement factor is greatly reduced in structures that are uniform in one of the dimensions. Since the structure considered here is essentially a two dimensional structure, we refer to this limit as the *2D bulk limit*.

In the case when the periodicity is close to the wavelength, the discreteness of the channels becomes important and (12) is no longer valid. Instead, as shown in Fig. 2c, the number of channels is

$$N = 2\left\lfloor \frac{k_0}{2\pi/L} \right\rfloor + 1 = 2\left\lfloor \frac{L}{\lambda} \right\rfloor + 1 \tag{15}$$

where $\lfloor x \rfloor$ represents the largest integer that is smaller than x. We further assume the medium has a high refractive index such that the following conditions are satisfied:

$$\begin{aligned} L &\gg \lambda/n, \\ d &\gg \lambda/n. \end{aligned} \tag{16}$$

Under these conditions, the resonance in the film can still be approximated as forming a continuum of states, and (13) is still applicable. The upper limit for the enhancement factor is thus calculated from (7), (13) and (15). In Fig. 2b, we plot such an upper limit as a function of normalized frequency

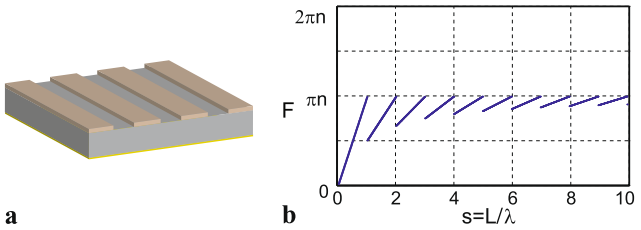

Fig. 3 (**a**) 1D grating structure with mirror symmetry. (**b**) Limit of absorption enhancement in grating structures with mirror symmetry

$s \equiv L/\lambda$. At low frequency, when $L/\lambda < 1$, there is only one channel, i.e. $N = 1$, while the number of resonances increases linearly with frequency. Hence the enhancement factor increases linearly with frequency, reaching its maximum value of $2\pi n$ at $L = \lambda$. At the frequency immediately above $s = 1$, the number of channels increases to $N = 3$, leading to a step-function drop of the enhancement factor. In general, such a sharp drop in enhancement factor occurs whenever new channels appear, i.e. whenever $L = m\lambda$, where m is an integer. Also, in between such sharp drops, the enhancement factor always increases as a function of frequency. In the limit of $L \gg \lambda$, the enhancement factor converges to the 2D bulk limit of πn.

We now analyze the effects of the symmetry of the grating profile on the light-trapping limit. In contrast to the asymmetrical grating profile shown in Fig. 2a, a symmetrical grating has mirror symmetry in the x-direction (Fig. 3a). Reference [32] proposes to use asymmetrical gratings to reduce the reflection in the normal direction, and thus increase the absorption. On the other hand, the semi-analytical method in Ref. [10] finds no difference for gratings with different symmetries. Here, we analyze the effect of structure symmetry on the fundamental limit of light absorption enhancement with our rigorous electromagnetic approach.

We first discuss the case of normally incident light. Due to mirror symmetry of the film, resonant modes either have an odd or even modal amplitude profile. The normally incident plane wave, which has even modal amplitude profile, cannot couple to modes with odd profiles. Therefore, for the symmetric case, the number of resonances that can contribute to the absorption is reduced by half when compared to the asymmetric case, i.e.:

$$M_{\text{sym}} = M/2 \tag{17}$$

where M is given by (13).

In the case where the period is smaller than the wavelength, there is only one channel $N_{\text{sym}} = N = 1$. Thus, when the period of the grating is less than the free-space wavelength, the symmetric case has a lower enhancement limit $F_{\text{sym}} = F/2$ (Fig. 3b).

When the period of the grating is larger than the wavelength, there are more channels, and we also need to consider the effect of symmetry on channels. Due to mirror symmetry, channels can be arranged as even and odd according to

$$\begin{aligned} S_{\text{even}} &= \frac{1}{\sqrt{2}}(S_{k_\parallel} + S_{-k_\parallel}) \\ S_{\text{odd}} &= \frac{1}{\sqrt{2}}(S_{k_\parallel} - S_{-k_\parallel}). \end{aligned} \tag{18}$$

Since the incident plane wave from the normal incidence has an even modal amplitude profile, only the even resonances can be excited, which only leak into even channels. Therefore, the number of channels available is also reduced by half $N_{\text{sym}} = N/2$ when $L \gg \lambda$. In this case, as seen in (7), we have the same enhancement limit as that of asymmetrical gratings $F_{\text{sym}} = F$ (Fig. 3b). Thus, the symmetry of the grating is important only when the periodicity of the grating is smaller or comparable to the wavelength of incident light. In structures with period much larger compared with the wavelength, the symmetry of the grating does not play a role in determining the upper limit of absorption enhancement.

The upper limit in a 1D grating structure falls far below the conventional bulk limit of $4n^2$ due to a reduced number of resonances. To achieve a higher enhancement factor, it is always better to use 2D gratings that are periodic in both x- and y-direction, since a 2D grating allows access to all resonances supported by a film. In the next section, we present a detailed discussion on the upper limit of light trapping with a 2D grating based on (7).

3.2 Theoretical upper limit of enhancement factor for 2D grating structures

We first consider the case where the grating has a square lattice, with a periodicity of L in both dimensions. In the frequency range $[\omega, \omega + \Delta\omega]$, assuming (16) is satisfied, the total number of guided resonances supported by the film is given by (8). Notice that the number of resonances increases quadratically as a function of frequency.

When a plane wave is normally incident upon the film, the grating can excite plane waves in other propagating directions in free space. The parallel wavevectors $G_{m,n}$ of these excited plane waves in free space are

$$G_{m,n} = m\frac{2\pi}{L}\hat{x} + n\frac{2\pi}{L}\hat{y}, \tag{19}$$

with m and n being integers. Hence these parallel wavevectors form a square lattice in the wavevector vector space (Fig. 4a, blue dots). Moreover, since these are propagating plane waves, their wavevectors need to lie within a circle as defined by $|G| < k_0 \equiv \frac{\omega}{c}$ (Fig. 4a, dashed line). The total number of different wavevector points, multiplied by two in order to take into account both polarizations, defines the

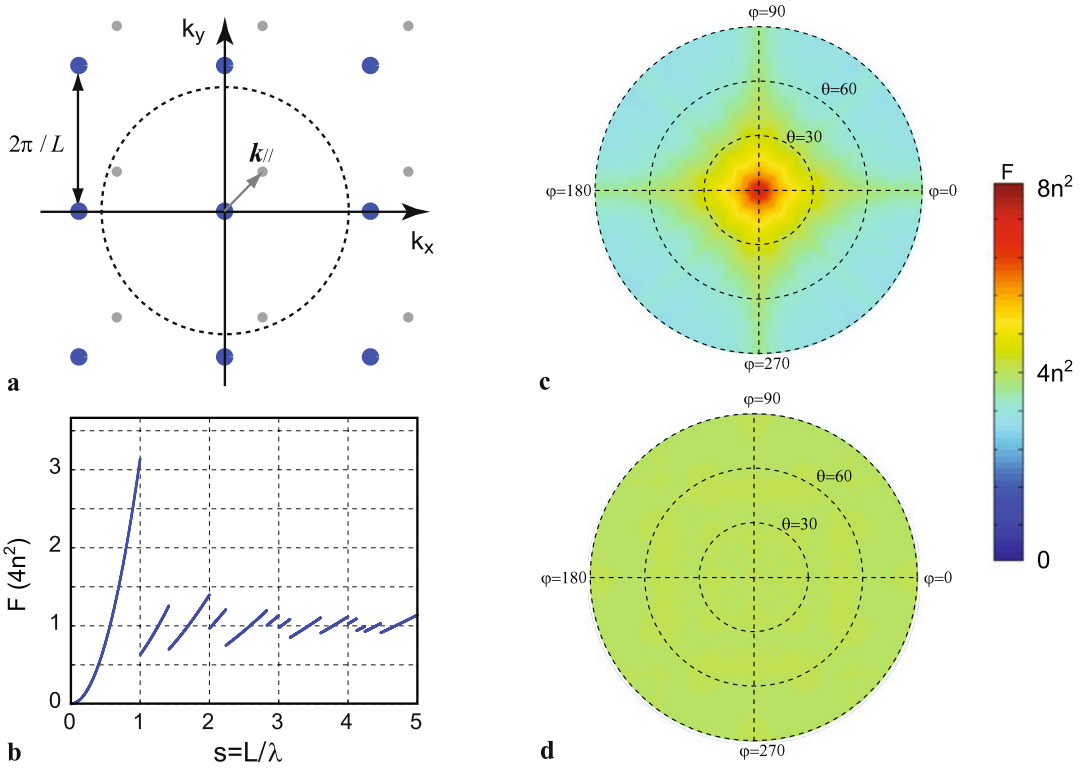

Fig. 4 (**a**) Channels in 2D k-space. *Blue* and *gray dots* represent channels when the incident light comes in from normal and off-normal directions, respectively. The radius of the circle is k_0. (**b**) Limit of absorption enhancement in 2D grating structures. (**c**) Angular response of the average enhancement factor integrated over wavelength from $\lambda = p$ to $\lambda = 2p$ for a grating with a periodicity of $L = p$. (**d**) The same as (**c**) except the periodicity is $L = 5p$

number of channels N that is required for the calculation using (7).

At low frequency when $s = L/\lambda < 1$, there are only two channels ($N = 2$), accounting for two polarizations, in the normal direction, while the number of resonances increases with frequency quadratically. Hence the enhancement factor increases quadratically with frequency and reaches its maximum value of $4\pi n^2$ at $s = 1$ (Fig. 4b). Immediately above $s = 1$, the wavelength becomes shorter than the period L. The number of channels increases to $N = 10$, leading to a step-function drop of the enhancement factor. In the limit of $L \gg \lambda$, the calculated upper limit reproduces the 3D bulk limit of $4n^2$ [24].

Next, we analyze the angular response of the upper limit of the enhancement factor by considering a plane wave incident from a direction specified by an incidence angle θ and an azimuthal angle φ. Such an incident plane wave has a parallel wavevector $k_\parallel = k_0 \sin(\theta)\cos(\varphi)\hat{x} + k_0 \sin(\theta)\sin(\varphi)\hat{y}$. In the presence of the grating, such a plane wave can excite other plane waves in free space with parallel wavevectors:

$$k = k_\parallel + G_{m,n}, \tag{20}$$

where $G_{m,n}$ is defined in (19), provided that these parallel wavevectors are located in a circle in k-space $|k| < k_0$, as is required for propagating plane waves.

In comparison to the normal incident case described by (19), (20) defines a similar square lattice in the wavevector space, except that the positions of the lattice points in k-space are now shifted by the parallel wavevector $k_\parallel$ of the incident plane wave (Fig. 4a). As a result of such a shift, one can see that the number of channels N, which is proportional to the number of k-space lattice points that fall within the circle of $|k| < k_0$, is dependent on the incidence angle. Such angular dependency is particularly strong for the case where there are only small numbers of channels, which occurs when the periodicity is about wavelength scale.

As an example, Fig. 4a illustrates the case where the normalized frequency $s = L/\lambda = 0.87 < 1$. For normal incidence, there is only one k-space lattice point (as shown by the blue dot in Fig. 4a) within the circle of $|k| < k_0$ (dashed line in Fig. 4a), corresponding to two channels. At the same frequency, for off-normal incident light with $k_\parallel = 0.3k_0\hat{x} + 0.3k_0\hat{y}$, corresponding to a plane wave incident from a direction as defined by $\theta = 25°$, $\varphi = 45°$, there are 3 k-space lattice points within the circle of $|k| < k_0$ (gray dots in Fig. 4a), and hence 6 available channels. Thus, for a

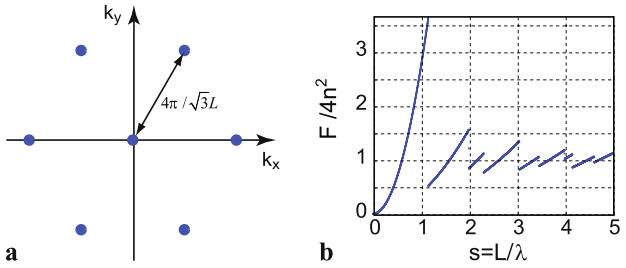

Fig. 5 (**a**) Channels in 2D k-space for a grating with triangular lattice periodicity. The lattice constant is L. (**b**) Upper limit of absorption enhancement for gratings with triangular lattice periodicity

plane wave incident from such an off-normal incident direction, the upper limit for absorption enhancement should be only 1/3 of the upper limit for normally incident light. This example illustrates that there can be substantial angular dependency in absorption enhancement when the periodicity is comparable to the wavelength. In contrast, when the periodicity is much larger than the wavelength, the k-space lattice points are densely distributed and the number of channels $N \gg 1$. Therefore, the shift of the lattice points in k-space due to different incidence angles has negligible effect on the total number of channels. In the case where $L \gg \lambda$, the upper limit of enhancement is not sensitive to the incidence angles.

In Fig. 4b, we provide detailed analytic results regarding the angular dependency of the upper limit of absorption enhancement. We consider a grating with a period $L = p$. For each direction of incidence as specified by an angle of incidence θ and an azimuthal angle of φ, we calculate the upper limit F at each frequency using (7). We then average the upper limit F calculated over the wavelength range between $\lambda = p$ to $\lambda = 2p$, and plot the spectral average $\overline{F}$ as a function of θ and φ in Fig. 4c. In this case, the grating period is smaller than the wavelength of interest. In the vicinity of the normal direction, $\overline{F}$ is approximately $8n^2$. Thus, it is possible to use a grating structure to obtain broad-band enhancement of absorption higher than $4n^2$ (Fig. 4c). This result is consistent with Fig. 4b: the wavelength range corresponds to a range of $0.5 \le s \le 1$, where the enhancement factor is above $4n^2$. However, when the incident light deviates from normal direction, $\overline{F}$ starts to drops (Fig. 4c). For incidence angles larger than 60°, $\overline{F}$ drops well below $4n^2$, showing a strong angular dependency.

As a second example, we consider the case where the period $L = 5p$ nm, and the same wavelength range, which for this grating periodicity corresponds to the normalized frequency range $2.5 \le s \le 5$. In this case, the period is considerably larger than the wavelength, and the number of channels is much larger than 1. The spectrally averaged upper limit of enhancement has much weaker angular dependency. As shown in Fig. 4d, $\overline{F}$ is around $4n^2$ for all incidence angles, showing a near-isotropic response.

Finally, we briefly comment on the influence of the lattice periodicity of the grating structure. The analysis above has focused on square lattices. In practice, a triangular lattice is often found in closely packed nanoparticles and nanowires [33]. For a grating with a triangular lattice with period L, the channels form a triangular lattice in k-space (Fig. 5a). The distance between the channel at the origin of k-space and its nearest neighbors is $k_T = (2/\sqrt{3})2\pi/L$, which is larger than that of the square lattice $k_S = 2\pi/L$. As a result, for normally incident light, the frequency range where the grating operates with only 2 channels is larger ($0 < s < 2/\sqrt{3}$) compared to the case of the square lattice ($0 < s < 1$). This leads to a higher maximum enhancement factor $8n^2\pi/\sqrt{3}$ (Fig. 5b). On the other hand, as the period becomes larger, the maximum enhancement ratios in gratings with different lattices all converge to the same bulk limit of $4n^2$.

To conclude this section on the theoretical analysis of 2D grating structures, we note that a grating with wavelength scale periodicity can achieve an absorption enhancement factor that is higher than $4n^2$ over a broad-range of wavelengths. Such enhancement, however, comes at the expense of substantial angular dependency. As a result, a grating structure in general, when the film thickness is a few wavelength thick, cannot overcome the conventional bulk limit of $4n^2/\sin^2\theta$. On the other hand, a grating structure with periodicity much larger than the wavelength has enhancement factor approaching $4n^2$ with near-isotropic response.

4 Nanophotonic light trapping beyond conventional limit

4.1 Light-trapping in thin films

We have described the light-trapping properties for films with thickness d much larger than the wavelength. In these situations, we use (8) to count the number of resonances in the films. When the thickness d of the film is comparable to half wavelength in material, one can reach the single-mode regime where the film supports a single waveguide mode band for each of the two polarizations. In such a case, (8) is no longer applicable. Instead, the number of resonances in the frequency range of $[\omega, \omega + \delta\omega]$ can be calculated as

$$M = 2 \times \frac{2\pi n_{wg}^2 \omega}{c^2} \left(\frac{L}{2\pi}\right)^2 \delta\omega \tag{21}$$

where the first factor of 2 arises from counting both polarizations. (Here, to facilitate the comparison to the standard conventional limit, for simplicity, we have assumed that the two polarizations have the same group index n_{wg}.) Notice that in this case the number of modes no longer explicitly depends upon the thickness d of the film.

In order to highlight the effect of such strong light confinement, we choose the periodicity to be a few wavelengths, in which case the number of channels can still be calculated using (9). As a result we obtain the upper limit for the absorption enhancement factor:

$$F = 2 \times 4n_{wg}^2 \frac{\lambda}{4n_{wg}d} V \tag{22}$$

where the factor $V = \frac{\alpha_{wg}}{\alpha_0}$ characterizes the overlapping between the profile of the guided mode and the absorptive active layer. α_{wg} and n_{wg} are the absorption coefficient and group index of the waveguide mode, respectively.

Equation (22) in fact becomes $4n^2$ in a dielectric waveguide of $d \approx \lambda/2n$. Therefore, reaching a single-mode regime is not sufficient to exceed the conventional limit. Instead, to achieve the full benefit of nanophotonics, one must either ensure that the modes exhibit deep-subwavelength-scale electric-field confinement, or enhance the group index to be substantially larger than the refractive index of the active material, over a substantial wavelength range. Below, using both exact numerical simulations and analytic theory, we will design geometries that simultaneously satisfy both these requirements.

4.2 Light-trapping enhancement beyond the classical limit using nanoscale modal confinement

Guided by the theory above, we now numerically demonstrate a nanophotonic scheme with an absorption enhancement factor significantly exceeding the conventional limit. We consider a thin absorbing film with a thickness of 5 nm (Fig. 6a), consisting of a material with a refractive index $n_L = \sqrt{2.5}$ and a wavelength-independent absorption length of 25 μm. The film is placed on a mirror that is approximated to be a perfect electric conductor (PEC). A PEC mirror is used for simulation convenience. In practice, it can be replaced by a dielectric cladding layer, which produces similar results [24]. Our aim here is to highlight the essential physics of nanophotonic absorption enhancement. The choice of material parameters therefore represents a simplification of actual material response. Nevertheless, we note that both the index and the absorption strength here are characteristic of typical organic photovoltaic absorbers in the weakly absorptive regime [34]. Furthermore, there is general interest in using thinner absorbers in organic solar cells given their short exciton diffusion lengths of about 3–10 nm [35–37].

In order to enhance the absorption in the active layer, we place a transparent cladding layer ($n_H = \sqrt{12.5}$) on top of the active layer. Such a cladding layer serves two purposes. First, it enhances density of state. The overall structure supports a fundamental mode with group index n_{wg} close to n_H, which is much higher than that of the absorbing material.

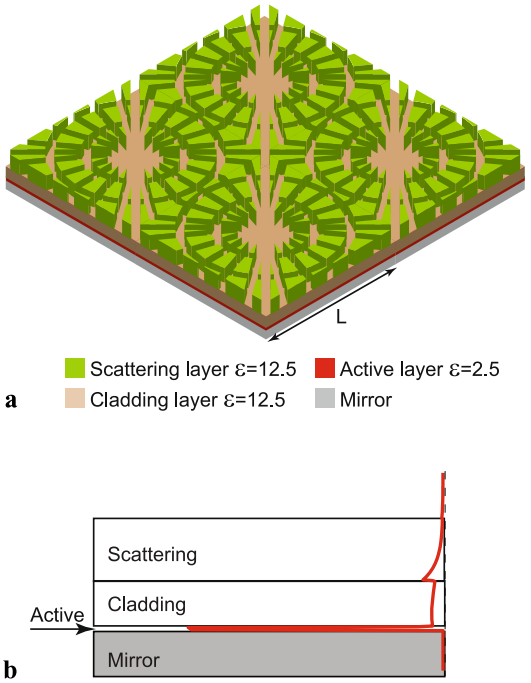

Fig. 6 Structure for overcoming the conventional light-trapping limit. (**a**) A nanophotonic light-trapping structure. The scattering layer consists of a square lattice of air groove patterns with periodicity $L = 1200$ nm. The thicknesses of the scattering, cladding, and active layers are 80 nm, 60 nm, and 5 nm, respectively. The mirror layer is a perfect electric conductor. (**b**) The profile of electric-field intensity for the fundamental waveguide mode. Fields are strongly confined in the active layer. To obtain the waveguide mode profile, the scattering layer is modeled by a uniform slab with an averaged dielectric constant

Second, the index contrast between active and cladding layer provides nanoscale field confinement. Figure 6b shows the fundamental waveguide mode. The field is highly concentrated in the low-index active layer, due to the well-known slot-waveguide effect [38]. Thus, the geometry here allows the creation of a broad-band high-index guided mode, with its energy highly concentrated in the active layer, satisfying the requirement in (22) for high absorption enhancement.

In order to couple incident light into such nanoscale guided modes, we introduce a scattering layer with a periodic pattern on top of the cladding layer, with a periodicity L much larger than our wavelength ranges of interest. Each unit cell consists of a number of air grooves. These grooves are oriented along different directions to ensure that scattering strength does not strongly depend on the angles and polarizations of the incident light. We emphasize that there is no stringent requirement on these grooves as long as the scattering strength dominates over resonance absorption rates.

We simulate the proposed structure by numerically solving Maxwell's equations (Fig. 7a). The device has a spectrally averaged absorption enhancement factor of $F = 119$ (red line) for normally incident light. (All the absorption

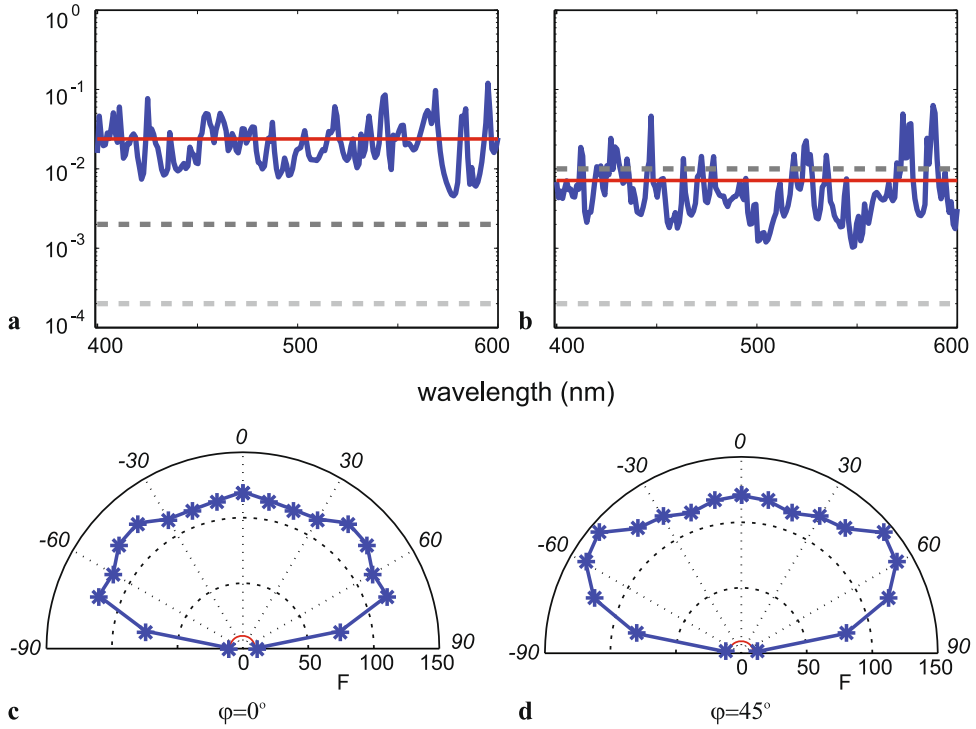

Fig. 7 Absorption of light-trapping structures. (**a**) Absorption spectrum for normally incident light for the structure shown in Fig. 6a. The spectrally averaged absorption (*red solid line*) is much higher than both the single-pass absorption (*light gray dashed line*) and the absorption as predicted by the limit of $4n_L^2$ (*dark gray dashed line*). The *vertical axis* is the absorption coefficient. (**b**) Absorption spectrum without nanoscale light confinement. The structure is the same as that of (**a**) except that the dielectric constant of the active layer is now the same as the cladding layer. The *dark gray dashed line* represents the absorption as predicted by the limit of $4n_H^2$. (**c**, **d**) Angular dependence of the spectrally averaged absorption enhancement factor for the structure in Fig. 6a. Incident angles are labeled on top of the semi-circles. Incident planes are oriented at 0 (**c**) and 45 (**d**) degrees (azimuthal angles) with respect to the [10] direction of the lattice. The *red circles* represent the $4n_L^2$ limit

spectra and enhancement factors are obtained by averaging s and p polarized incident light.) This is well above the conventional limit for both the active material ($4n_L^2 = 10$) and the cladding material ($4n_H^2 = 50$). Moreover, the angular response is nearly isotropic (Fig. 7c, d). Thus such enhancement cannot be attributed to the narrowing of angular range in the emission cone, and instead is due entirely to the nanoscale field confinement effect.

Using our theory, we calculate the theoretical upper limit of light-trapping enhancement in this structure [24]. For wavelength $\lambda = 500$ nm, we obtain an upper limit of $F = 147$. The enhancement factor observed in the simulation is thus consistent with this predicted upper limit. The actual enhancement factor obtained for this structure falls below the calculated theoretical upper limit because some of the resonances are not in the strong over-coupling regime.

To illustrate the importance of nanoscale field confinement enabled by the slot-waveguide effect, we change the index of the material in the absorptive layer to n_H. Such a structure does not exhibit the slot-waveguide effect. The average enhancement in this case is only 37, falling below the conventional limit of 50 (Fig. 7b).

4.3 Light-trapping for infinitesimal inclusions

The microscopic physics of the enhancement in the numerical example above is related to the Lorentz local field effect (34). In this section, using (6), we provide an analytic expression capturing the effect of local field enhancement on light trapping. To obtain a close-form analytic result, we examine a small inclusion with a relevant dimension at a deep sub-wavelength scale, of a lossy material with a low index n_L and a small absorption coefficient α_0, embedded in a lossless bulk medium with high index n_H. We study the effect of absorption enhancement when light trapping is performed on the bulk, by, for example, roughening the bulk-air interface (Fig. 8). To facilitate the computation, we assume a periodic boundary condition in the xy-plane with a large periodicity L, and a thickness of D for the bulk medium.

To apply (6), we first calculate the intrinsic loss rate $\gamma_{i,m}$ of the mth resonance mode having a modal electric field $\vec{E}_m(\vec{r})$:

$$\gamma_{i,m} = \frac{\alpha_0 n_L}{c} \frac{\int_{\text{inclusion}} n_L^2 |\vec{E}_m(\vec{r})|^2 \, d\vec{r}}{\int n^2(\vec{r}) |\vec{E}_m(\vec{r})|^2 \, d\vec{r}}. \tag{23}$$

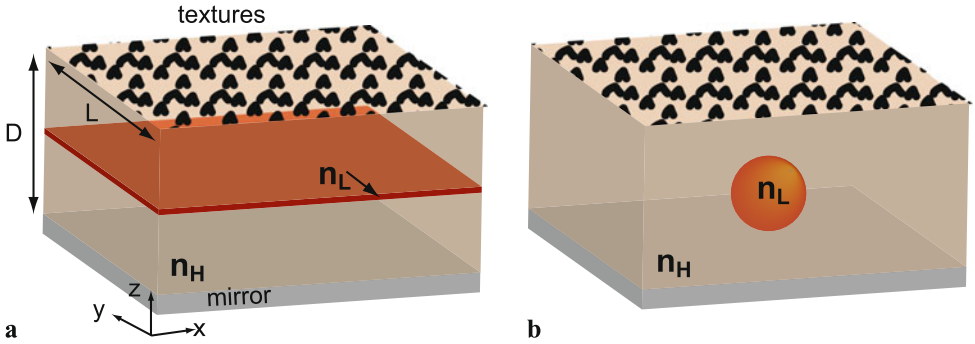

Fig. 8 Illustration of a small active region embedded in a bulk host material. (**a**) A thin layer; and (**b**) a spherical inclusion

Since the inclusion is small, the field $\vec{E}_m(\vec{r})$ can be derived from a corresponding plane wave mode in a uniform bulk medium with an electric field $\vec{E}_m(\vec{r}) = \vec{E}_m^0 e^{i\vec{k}_m\cdot\vec{r}}$ having an amplitude $|\vec{E}_m^0| = E_0$. Outside the inclusion region, we assume $\vec{E}_m(\vec{r}) = \vec{E}_m^0(\vec{r})$. The denominator in (13) thus becomes

$$\int n^2(\vec{r})\left|\vec{E}_m(\vec{r})\right|^2 d\vec{r} \approx n_H^2 E_0^2 L^2 D. \tag{24}$$

Inside the inclusion, the electric fields $\vec{E}_m(\vec{r})$ can be determined by boundary conditions.

We consider the structure in Fig. 5a first, where a thin lossy layer perpendicular to the z-axis, of a thickness d, is embedded in the high-index bulk. Inside the thin layer, applying the electric-field boundary condition, we have

$$\vec{E}_m(\vec{r}) = E_{x,m}^0(\vec{r})\hat{x} + E_{y,m}^0(\vec{r})\hat{y} + \left(\frac{n_H^2}{n_L^2}\right)E_{z,m}^0(\vec{r})\hat{z}. \tag{25}$$

Combining (23), (24), and (25), we therefore have

$$\gamma_{i,m} = \frac{\alpha_0 c}{n_L}\frac{n_L^2\left(|E_{x,m}^0|^2 + |E_{y,m}^0|^2 + \frac{n_H^2}{n_L^2}|E_{z,m}^0|^2\right)}{n_H^2 E_0^2}\frac{d}{D}. \tag{26}$$

Thus, the enhancement ratio becomes

$$F = \frac{1}{\alpha_0 d}\cdot\frac{2\pi}{\Delta\omega}\cdot\frac{\sum_m \gamma_{i,m}}{N} = 4n_L^2\left(\frac{2}{3}\frac{n_H}{n_L} + \frac{1}{3}\frac{n_H^5}{n_L^5}\right). \tag{27}$$

In deriving (27), we note that

$$\sum_m |E_{x,m}|^2 = \sum_m |E_{y,m}|^2 = \sum_m |E_{z,m}|^2 = \frac{1}{3}ME_0^2. \tag{28}$$

We also use the relation $\frac{2\pi}{\Delta\omega}\frac{M}{N}\cdot\frac{\alpha_0 n_H}{c} = 4n_H^2\alpha_0 D$, as derived in a previous section (see (10)).

Equation (27) is consistent with [39]. Our theoretical framework, however, is very general and allows us to treat many other light-trapping scenarios as well. As another example (Fig. 8b), we calculate the light-trapping enhancement factor for a small spherical inclusion having a volume V_s embedded in a bulk medium, by noting that inside the sphere, the field is [40]

$$\left|\vec{E}_m(r)\right| = \frac{3n_H^2}{2n_H^2 + n_L^2}E_0. \tag{29}$$

Following the same procedure as outlined above from the thin layer case, we have an absorption enhancement factor of

$$F_{\text{sphere}} = 4n_L^2\frac{9n_H^5/n_L^5}{(2n_H^2/n_L^2 + 1)^2} \tag{30}$$

when compared the single-pass absorption rate of a sphere of $\alpha V_s/L^2$.

The analytic results thus show that embedding low-index absorptive inclusions in a high-index medium can significantly enhance light absorption beyond the conventional limit, in consistency with the numerical results of the previous section. The combination of wave effects with the local field effects may provide significant flexibilities for design of light absorption enhancement, with potentials for even higher absorption enhancement factor.

5 Conclusion

We have developed a statistical coupled-mode theory for nanophotonic light trapping, and shown that properly designed nanophotonic structures can achieve enhancement factors that far exceed the conventional limit. Our results presented here indicate substantial opportunity for nanophotonic light-trapping using only low-loss dielectric components. The basic theory moreover, is generally applicable to any photonic structure, including nanowire [41, 42] and plasmonic structures [43]. In plasmonic structures in particular, the presence of nanoscale guided modes may also provide opportunities to overcome the conventional limit.

References

1. K. Taretto, U. Rau, Modeling extremely thin absorber solar cells for optimized design. Prog. Photovolt. **12**, 573–591 (2004)

2. E. Yablonovitch, Statistical ray optics. J. Opt. Soc. Am. A **72**, 899–907 (1982)
3. A. Goetzberger, Optical confinement in thin Si-solar cells by diffuse back reflectors, in *Fifteenth IEEE Photovoltaic Specialists Conference - 1981* (IEEE Press, New York, 1981), pp. 867–870
4. P. Campbell, M.A. Green, The limiting efficiency of silicon solar-cells under concentrated sunlight. IEEE Trans. Electron Devices **33**, 234–239 (1986)
5. P. Sheng, A.N. Bloch, R.S. Stepleman, Wavelength-selective absorption enhancement in thin-film solar cells. Appl. Phys. Lett. **43**, 579–581 (1983)
6. P. Bermel, C. Luo, L. Zeng, L.C. Kimerling, J.D. Joannopoulos, Improving thin-film crystalline silicon solar cell efficiencies with photonic crystals. Opt. Express **15**, 16986–17000 (2007)
7. L. Hu, G. Chen, Analysis of optical absorption in silicon nanowire arrays for photovoltaic applications. Nano Lett. **7**, 3249–3252 (2007)
8. A. Chutinan, S. John, Light trapping and absorption optimization in certain thin-film photonic crystal architectures. Phys. Rev. A **78**(2), 023825 (2008)
9. H.R. Stuart, D.G. Hall, Thermodynamic limit to light trapping in thin planar structures. J. Opt. Soc. Am. A **14**, 3001–3008 (1997)
10. I. Tobias, A. Luque, A. Marti, Light intensity enhancement by diffracting structures in solar cells. J. Appl. Phys. **104**, 034502 (2008)
11. P.N. Saeta, V.E. Ferry, D. Pacifici, J.N. Munday, H.A. Atwater, How much can guided modes enhance absorption in thin solar cells? Opt. Express **17**, 20975–20990 (2009)
12. R.A. Pala, J. White, E. Barnard, J. Liu, M.L. Brongersma, Design of plasmonic thin-film solar cells with broadband absorption enhancements. Adv. Mater. **21**, 3504–3509 (2009)
13. S.B. Mallick, M. Agrawal, P. Peumans, Optimal light trapping in ultra-thin photonic crystal crystalline silicon solar cells. Opt. Express **18**, 5691–5706 (2010)
14. C. Lin, M.L. Povinelli, Optical absorption enhancement in silicon nanowire arrays with a large lattice constant for photovoltaic applications. Opt. Express **17**, 19371–19381 (2009)
15. S. Mokkapati, F.J. Beck, A. Polman, K.R. Catchpole, Designing periodic arrays of metal nanoparticles for light-trapping applications in solar cells. Appl. Phys. Lett. **95**, 053115 (2009)
16. J. Müller, B. Rech, J. Springer, M. Vanecek, TCO and light trapping in silicon thin film solar cells. Sol. Energy **77**, 917–930 (2004)
17. M.D. Kelzenberg, S.W. Boettcher, J.A. Petykiewicz, D.B. Turner-Evans, M.C. Putnam, E.L. Warren, J.M. Spurgeon, R.M. Briggs, N.S. Lewis, H.A. Atwater, Enhanced absorption and carrier collection in Si wire arrays for photovoltaic applications. Nat. Mater. **9**, 239–244 (2010)
18. E. Garnett, P. Yang, Light trapping in silicon nanowire solar cells. Nano Lett. **10**, 1082–1087 (2010)
19. S. Pillai, K.R. Catchpole, T. Trupke, M.A. Green, Surface plasmon enhanced silicon solar cells. J. Appl. Phys. **101**, 093105 (2007)
20. L. Zeng, Y. Yi, C. Hong, J. Liu, N. Feng, X. Duan, L.C. Kimerling, B.A. Alamariu, Efficiency enhancement in Si solar cells by textured photonic crystal back reflector. Appl. Phys. Lett. **89**, 111111 (2006)
21. L. Tsakalakos, J. Balch, J. Fronheiser, B.A. Korevaar, O. Sulima, J. Rand, Silicon nanowire solar cells. Appl. Phys. Lett. **91**, 233117 (2007)
22. C. Rockstuhl, F. Lederer, K. Bittkau, R. Carius, Light localization at randomly textured surfaces for solar-cell applications. Appl. Phys. Lett. **91** (2007)
23. J. Zhu, Z. Yu, G.F. Burkhard, C.-M. Hsu, S.T. Connor, Y. Xu, Q. Wang, M. McGehee, S. Fan, Y. Cui, Optical absorption enhancement in amorphous silicon nanowire and nanocone arrays. Nano Lett. **9**, 279–282 (2008)
24. Z. Yu, A. Raman, S. Fan, Fundamental limit of nanophotonic light trapping for solar cells. Proc. Natl. Acad. Sci. USA **107**, 17491–17496 (2010)
25. Z. Yu, A. Raman, S. Fan, Fundamental limit for light trapping in grating structures. Opt. Express (2010)
26. Z. Yu, S. Fan, Angular constraint on light-trapping absorption enhancement in solar cells. Appl. Phys. Lett. **98**, 011106 (2011)
27. P.W. Anderson, Absence of diffusion in certain random lattices. Phys. Rev. **109**, 1492 (1958)
28. S. Fan, J.D. Joannopoulos, Analysis of guided resonances in photonic crystal slabs. Phys. Rev. B **65**, 235112 (2002)
29. H.A. Haus, *Waves and Fields in Optoelectronics*. Prentice-Hall Series in Solid State Physical Electronics (Prentice-Hall, Englewood Cliffs, 1984), pp. xii, 402 p.
30. S. Fan, W. Suh, J.D. Joannopoulos, Temporal coupled-mode theory for the Fano resonance in optical resonators. J. Opt. Soc. Am. A **20**, 569–572 (2003)
31. C. Kittel, *Introduction to Solid State Physics*, 7th edn. (Wiley, New York, 1995), p. 699
32. C. Heine, R.H. Morf, Submicrometer gratings for solar energy applications. Appl. Opt. **34**, 2476–2482 (1995)
33. J. Zhu, C.-M. Hsu, Z. Yu, S. Fan, Y. Cui, Nanodome solar cells with efficient light management and self-cleaning. Nano Lett. **10**, 1979–1984 (2009)
34. H. Hoppe, N.S. Sariciftci, Organic solar cells: An overview. J. Mater. Res. **19**, 1924–1945 (2004)
35. A. Mayera, S. Scullya, B. Hardina, M. Rowella, M. McGeheea, Polymer-based solar cells. Mater. Today **10**, 28–33 (2007)
36. W.U. Huynh, J.J. Dittmer, A.P. Alivisatos, Hybrid nanorod-polymer solar cells. Science **295**, 2425–2427 (2002)
37. G. Yu, J. Gao, J.C. Hummelen, F. Wudl, A.J. Heeger, Polymer photovoltaic cells: enhanced efficiencies via a network of internal donor-acceptor heterojunctions. Science **270**, 1789–1791 (1995)
38. V.R. Almeida, Q. Xu, C.A. Barrios, M. Lipson, Guiding and confining light in void nanostructure. Opt. Lett. **29**, 1209–1211 (2004)
39. M.A. Green, Enhanced evanescent mode light trapping in organic solar cells and other low index optoelectronic devices. Progr. Photovol. (2010)
40. J.D. Jackson, *Classical Electrodynamics* (Wiley, New York, 1998)
41. M. Law, L.E. Greene, J.C. Johnson, R. Saykally, P. Yang, Nanowire dye-sensitized solar cells. Nat. Mater. **4**, 455–459 (2005)
42. B.M. Kayes, H.A. Atwater, N.S. Lewis, Comparison of the device physics principles of planar and radial p-n junction nanorod solar cells. J. Appl. Phys. **97**, 114302 (2005)
43. H.A. Atwater, A. Polman, Plasmonics for improved photovoltaic devices. Nat. Mater. **9**, 205–213 (2010)